Dosimetry characterization of a multibeam radiotherapy treatment for age-related macular degeneration

Choonsik Lee
Department of Nuclear and Radiological Engineering, University of Florida, Gainesville, Florida 32611

Erik Chell, Michael Gertner, and Steven Hansen
Oraya Therapeutics, Inc., Newark, California 94560

Roger W. Howell
Department of Radiology, University of Medicine and Dentistry of New Jersey, Newark, New Jersey 07103

Justin Hanlon
Department of Nuclear and Radiological Engineering, University of Florida, Gainesville, Florida 32611

Wesley E. Bolch[a)]
Departments of Nuclear and Radiological and Biomedical Engineering, University of Florida, Gainesville, Florida 32611

(Received 19 May 2008; revised 7 August 2008; accepted for publication 8 September 2008; published 23 October 2008)

Age-related macular degeneration (ARMD) is a major health problem worldwide. Advanced ARMD, which ultimately leads to profound vision loss, has dry and wet forms, which account for 20% and 80% of cases involving severe vision loss, respectively. A new device and approach for radiation treatment of ARMD has been recently developed by Oraya Therapeutics, Inc. (Newark, CA). The goal of the present study is to provide a initial dosimetry characterization of the proposed radiotherapy treatment via Monte Carlo radiation transport simulation. A 3D eye model including cornea, anterior chamber, lens, orbit, fat, sclera, choroid, retina, vitreous, macula, and optic nerve was carefully designed. The eye model was imported into the MCNPX2.5 Monte Carlo code and radiation transport simulations were undertaken to obtain absorbed doses and dose volume histograms (DVH) to targeted and nontargeted structures within the eye. Three different studies were undertaken to investigate (1) available beam angles that maximized the dose to the macula target tissue, simultaneously minimizing dose to normal tissues, (2) the energy dependency of the DVH for different x-ray energies (80, 100, and 120 kVp), and (3) the optimal focal spot size among options of 0.0, 0.4, 1.0, and 5.5 mm. All results were scaled to give 8 Gy to the macula volume, which is the current treatment requirement. Eight beam treatment angles are currently under investigation. In all eight beam angles, the source-to-target distance is 13 cm, and the polar angle of entry is 30° from the geometric axis of the eye. The azimuthal angle changes in eight increments of 45° in a clockwise fashion, such that an azimuthal angle of 0° corresponds to the 12 o'clock position when viewing the treated eye. Based on considerations of nontarget tissue avoidance, as well as facial-anatomical restrictions on beam delivery, treatment azimuthal angles between 135° and 225° would be available for this treatment system (i.e., directly upward and entering the eye from below). At beam directions approaching 225° and higher, some dose contribution to the optic nerve would result under the assumption that the optic nerve is tilted cranially above the geometric axis in a given patient, a feature not typically seen in past studies. A total treatment dose of 24 Gy would be delivered in three 8 Gy treatments at these selected azimuthal angles. Dose coefficients, defined as the macula radiation absorbed dose per unit air kerma in units of Gy/Gy, were 16% higher for 120 kVp x-ray beams in comparison to those at 80 kVp, thus requiring only 86% of the integrated tube current (mAs) for equivalent dose delivery. When 0.0, 0.4, and 1.0 mm focal spot sizes were used, the dose profiles in the macula are very similar and relatively uniform, whereas a 5.5 mm focal spot size produced a more nonuniform dose profile. The results of this study demonstrate the therapeutic promise of this device and provide important information for further design and clinical implementation for radiotherapy treatments for ARMD. [DOI: 10.1118/1.2990780]

Key words: age-related macular degeneration, radiation treatment, Monte Carlo method, eye phantom, dose volume histogram

I. INTRODUCTION

Age-related macular degeneration (ARMD) is a major health problem worldwide. Advanced ARMD, which ultimately leads to profound vision loss, has dry and wet forms.[1,2] The dry (atrophic) form accounts for about 20% of all cases involving severe visual loss. This form entails atrophy of the retinal pigment epithelial layer below the retina. As a consequence, there is loss of rods and cones in the central portion of the eye that ultimately leads to vision loss. The wet (neovascular) form accounts for 80% of all cases involving severe vision loss.[1,3] The wet form begins with the formation of fibrovascular tissue from the choroids through the Bruch's membrane. This choroidal neovascularization grows beneath the pigment epithelium or into the sensory retina. As a consequence, there is often leakage and bleeding from the vessels that, in turn, leads to increased tension at the macular lesion, with corresponding severe loss of vision.

There is no current treatment option for dry ARMD and so physicians usually monitor dry ARMD for the first signs that it is progressing to the more dangerous wet ARMD; however, vitamin supplements have been shown to be helpful in this regard.[4] Therapeutic options for wet ARMD include laser photocoagulation,[5] photodynamic therapy (PDT) using verteporfin (Visudyne®, Novartis, Basil, Switzerland),[6] and intraocular drug therapy with ranibizumab (Lucentis®, Genentech, San Francisco, CA)[7] or pegaptanib sodium (Macugen®, OSI-Eyetech, New York, NY).[8] Laser photocoagulation for wet ARMD is the oldest form of treatment dating to the early 1980s. This treatment worked well in reducing chorodial neovascular membrane formation, but the therapy rendered scaring of the macula with permanent loss of central vision. PDT treatment reduces moderate visual loss, but only a few subjects demonstrated improved vision; consequently, this treatment has also been abandoned. Further, for intraocular drug treatments, patients should receive periodical injections, which have significant drawbacks. As a result, alternative therapy options without budgetary burdens of repeated visits, injection fees, and pharmaceutical costs are sought by the medical community.

Clinical trials are underway for two radiation therapy options. The Therasight™ ocular brachytherapy system (Theragenics, Buford, GA) utilizes low-energy x-rays emitted by a ^{103}Pd radioactive source to provide high-dose-rate irradiation of the macula.[9] In this approach, a three-clock-hour conjunctival peritomy at the limbus is performed and the superotemporal quadrant is bluntly dissected. Muscle hooks are used to gently retract the lateral and superior rectus muscles. The applicator and its sterile sheath are then inserted under the macula using an image-guided technique and the shield that covers the radioactive portion of the applicator is retracted to permit macular irradiation.[10] The Epi-Rad90™ Ophthalmic System (NeoVista, Fremont, CA) treats neovascularization of retinal tissue by means of a focal, directional delivery of beta particles emitted by ^{90}Sr to the target tissues in the retina. The NeoVista Study Group presented an impressive clinical study where a total of 27 patients with subfoveal choroidal neovascularization (CNV) were enrolled.[11] They were treated with a targeted radiation dose of 24 Gy using the Epi-Rad90 Opthalmic System and two intravitreal injections of bevacizumab. At 12 months, 48% of the patients achieved gains $\geqslant$3 lines and 96% achieved stable or improved vision.

Additionally, the use of proton therapy, gamma knife radiosurgery (GKS), and external beam radiotherapy have been reported for ARMD treatment by some authors.[12–18] An analysis of patients treated with proton therapy was conducted in which the authors deemed this treatment option unacceptable due to the high risk of radiation retinopathy.[12] Another study using GKS included ten patients with CNV treated via a single-fraction 10 Gy dose to the macula.[13] One year later, six of the patients had remained stable, whereas four had decreased vision, and six had shown growth in the neovasculature. There have been a number of clinical studies involving the use of external beam radiotherapy as a possible nonsurgical treatment or ARMD where 10–20 Gy is delivered to the macula in 2–3 Gy fractions.[19] Some have produced results of reduction in vision loss, whereas others have failed to show any benefit, and in some cases have shown deleterious effects, such as cataract formation and xerophthalmia. Nevertheless, there have been sufficient pilot clinical studies to suggest that photon radiotherapy may be a viable option to treat ARMD if higher fractions (>4 Gy) can be applied to the macula target, simultaneously limiting nontarget tissue toxicity.

The biological response of the human eye to ionizing radiation is well documented. A review of the major findings may be found in Section 5 of Report No. 130 of the National Council on Radiation Protection and Measurement (NCRP).[20] Much of the experience on the radiation response of the eye derives from studies with fractionated and chronic regimens of low-LET radiation. The radiation absorbed doses that produce minimally detectable changes or functional disabilities are 6, 5, 30, 15, 16, 2, and 25 Gy, for the lid, conjunctiva, cornea, sclera, iris, lens, and retina, respectively.[20] These are conservative dose estimates that err in the direction of greater radiological protection. The corresponding visually debilitating absorbed doses to these same ocular structures are 40, 35, 30, 200, 16, 5.5, and 25 Gy, respectively.[20]

The radiosensitivity of the optic nerve, which is one of the more important nontarget tissues, has been studied in patients whose optic nerve was unavoidably or unintentionally irradiated as a consequence of brain or head tumor radiotherapy. Optic nerve mean doses as low as 8 Gy were found to be deleterious.[21] However, others have found that point doses of up to 12 Gy to the anterior optic pathway (nerve or chiasm) resulted in a low risk of developing clinically symptomatic radiation-induced optic neuropathy.[22]

Considering that current proton therapy options remain controversial, and clinical photon therapy trails have shown some positive results with deliveries of 2–3 Gy fractions, a new device for radiation treatment of ARMD with higher dose fractions is in development by Oraya Therapeutics, Inc. Preliminary data recently obtained in an mini-pig animal model show that stereotactic radiosurgery can be accom-

plished without adverse events.[23] To provide information for refining the design of this treatment device, a dosimetry characterization study was undertaken using Monte Carlo radiation transport simulation. A 3D eye model including cornea, anterior chamber, lens, orbit, fat, sclera, choroid, retina, vitreous, macula, and optic nerve was carefully designed based on the standard anatomy and dimensional data reported in NCRP Report No. 130.[20] The eye model was imported to the MCNPX2.5 Monte Carlo code[24] and radiation transport simulations were performed to investigate absorbed doses and dose volume histograms (DVH) to target and nontarget tissues within the eye model. Dosimetry for macula, optic nerve, and lens was characterized for different optic nerve tilt angles (cranial-caudal direction), x-ray beam energies, and focal spot sizes to further refine combinations of preferred treatment techniques.

II. MATERIALS AND METHODS

II.A. Monte Carlo radiation transport code MCNPX

Computational models of both the eye and its substructures, as well as the simulations of ocular radiotherapy of ARMD, were performed using the MCNPX version 2.5.0 radiation transport code developed at Los Alamos National Laboratory.[24] MCNPX is a general purpose Monte Carlo radiation transport code that tracks x-ray photons and their secondary electrons within user-defined geometrical regions, tissue compositions, and across a broad range of particle energies. The combinatorial geometry features of MCNPX provided an efficient method of modeling the detailed anatomical features of the eye and its targeted and nontargeted substructures. Sampling histories ranged from 10^6 for mean estimates of tissue absorbed dose, whereas 10^7 photon histories were considered for mesh tally calculations needed for construction of dose volume histograms.

II.B. X-ray source model

MCNPX requires the energy spectra of the x-ray tube defined as a plot of the fractional number of photons emitted as a function of photon energy. For this purpose, we have employed a computer program described in Report No. 78 of the Institute of Physics and Engineering in Medicine.[25] The program generates simulated x-ray emission spectra for tungsten anode tubes operated between 80 and 120 kVp and for total Al filtration 2 mm. Other parameters include the voltage ripple (assumed in this study to be 0% for high frequency generators) and the anode angle (assumed in this study to be 12°). Figure 1(a) 2 mm of Al. Using the simulated x-ray energy spectra, a divergent x-ray beam was modeled in MCNPX with a point source coupled with an angle biasing technique provided in the MCNPX code structure. The divergence angle was set so that the x-ray beam completely encompassed the 4 mm diameter of the macula target within the back of the eye. As demonstrated in Fig. 1(b), it was found that inclusion of secondary electron transport did not significantly alter values of tissue dose assessed under the kerma approximation. Consequently, at the photon energies considered in this study (80–120 kVp x-ray spectra), secondary electron transport was not performed for computational efficiency.

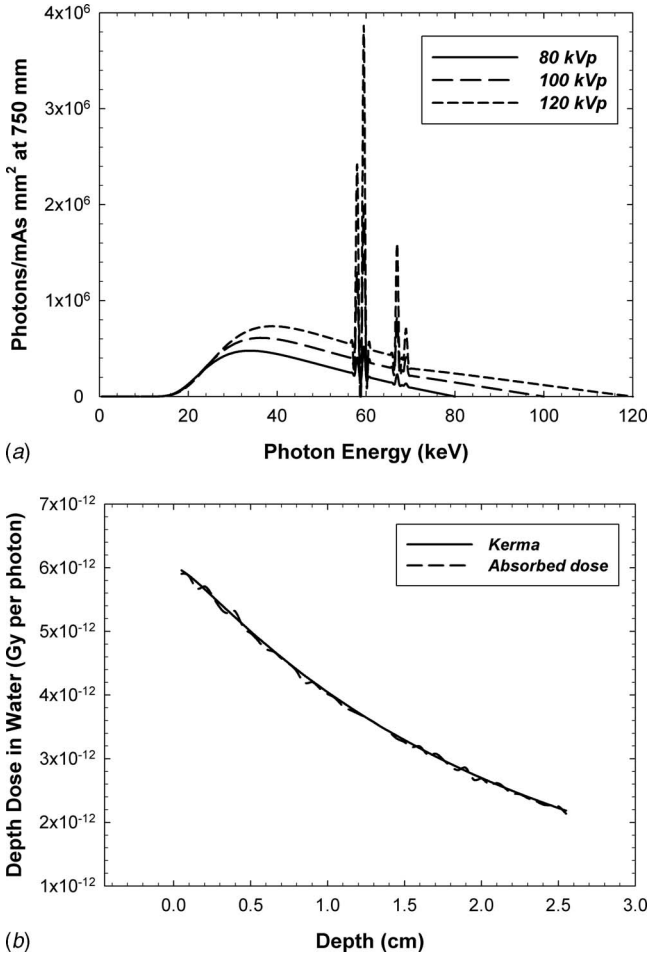

FIG. 1. (a) Photon energy spectra at 80, 100, and 120 kVp at a total filtration of 2 mm Al as generated from spectrum processor of IPEM Report 78. (b) Percent depth dose in water with (absorbed dose) and without (kerma) secondary electron transport for the 120 kVp spectrum. Kerma depth dose (solid line) was generated using 10^6 histories, whereas 10^8 histories were required for the absorbed dose (dashed line) values.

II.C. Geometrical model of the eye and its substructures

A reference eye model for radiation transport simulations was adopted from the dimensions given in Fig. 5.5 of NCRP Report No. 130.[20] The spatial dimensions of the various structures, and their relative positions, are provided in Fig. 2(A). In this initial dosimetric model, constructed for proof-of-principle calculations, we have assumed a symmetric ocular geometry, such that the geometric axis (center of lens to center of posterior curvature of the eye) is equivalent to the visual axis (center of lens to center of macula). In reality, these axes are slightly different (macula is positioned slightly off the geometric axis), yet definitive values for this shift are currently under investigation and will be addressed in subsequent versions of the model.

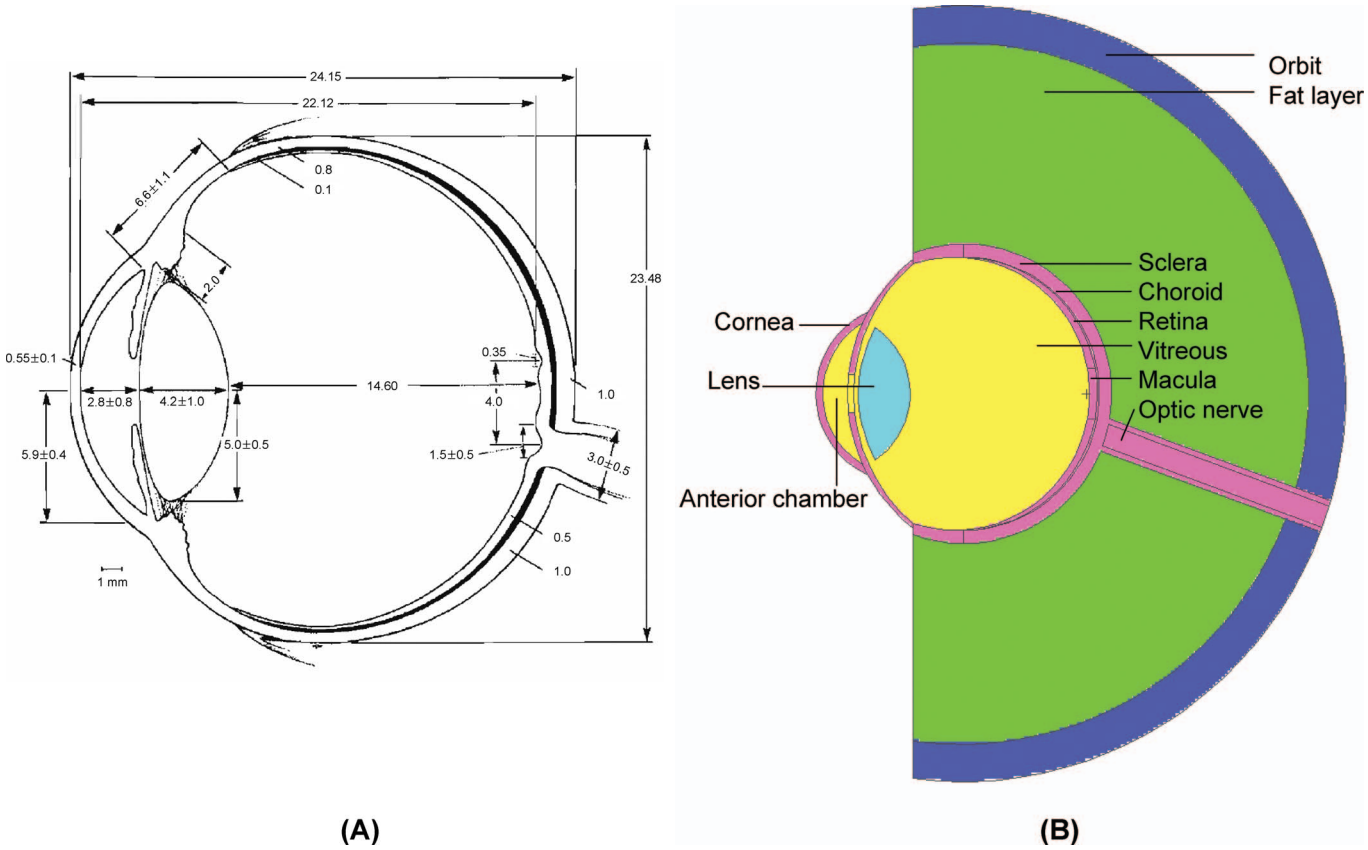

FIG. 2. (**A**) Dimensions and locations of tissue structures within the human eye (sagittal cross section) as provided in NCRP Report No. 130 (all dimensions are in mm). (**B**) Final MCNPX geometrical eye model (patient's right eye in transverse cross section). The macula target is defined as a puckered disk within the retina at a diameter of 4 mm.

Each substructure of interest was modeled through combinatorial geometry as a series of overlapping spheres or spherical shells, with Boolean logic operators used in MCNPX2.5 to include or exclude portions of a given sphere that define each tissue region. The final MCNPX geometrical model is shown in Fig. 2(B). The target region—the macula—is modeled as a disk-like structure 4 mm in diameter situated within the retina. As the retina is modeled as a spherical shell at the back of the eye, the macula is therefore more of a puckered disk in the current model. The optic nerve is currently modeled as a cylindrical cuboid structure tilted inward (medially) by 20° (as indicated in NCRP Report No. 130) and tilted vertically (cranial-caudal direction) by a variable angle ranging from −20° (maximal caudal tilt) to 0° (horizontally aligned within the geometric axis) to +20° (maximal cranial tilt). The optic nerve as shown in Fig. 2 is positioned in an assumed rotational position, yet in reality can rotate around the geometric axis (the subject of further work). Six different elemental tissue compositions were used within the MCNPX model as given in Table I: soft tissue, homogeneous skeleton, adipose tissue, lens, water, and air. Elemental tissue compositions were taken from those given in ORNL/TM-8381 and ICRU Report 46—reference standards for radiation transport studies in human tissues.[26,27]

TABLE I. Material and density assignments to substructures within the 3D MCNPX eye model with corresponding literature sources.

Materials	Organ/region	Density (g/cm^3)	Comment
Soft tissue	Cornea, sclera, choroid, retina, and macula	1.04	Soft tissue (ORNL TM-8381—Table A-1)
Homogeneous skeleton	Orbit	1.40	Skeleton (ORNL TM-8381—Table A-1)
Adipose tissue	Fat layer	0.95	Adipose tissue (ICRU 46—Adult #2)
Lens	Lens	1.07	Eye lens (ICRU 46—Adult)
Water	Anterior chamber and vitreous body	1.00	
Air	Surrounding region	0.0012	

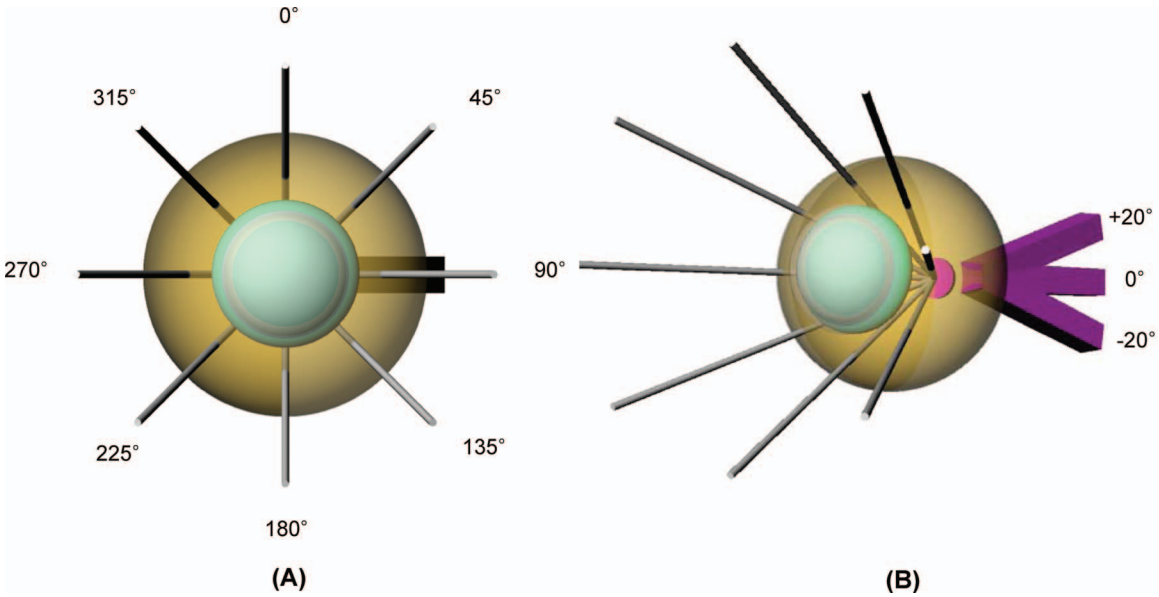

FIG. 3. Graphical representations of 8 possible radiotherapy beam entry directions for treatment of ARMD in (**A**) frontal and (**B**) perspective views. Beam 0° is directed caudally (downward) within the medial plane of the treated eye, whereas beam 180° is directed cranially (upward). A cylindrical cuboidal optic nerve model is situated right behind the puckered-shaped macula target. Its vertical tilt angle is allowed to vary from −20° to +20°, from the horizontal visual axis.

II.D. Irradiation geometry

The radiotherapy treatment should avoid direct irradiation of the lens. Thus, a beam angle of incidence that targets the macula without passing through the lens is required. This angle (called the polar angle and measured relative to the geometric axis) should be no smaller than would be required to miss the lens given the beam diameter, and should be no greater than that defined by the orbit bone. For a fixed polar angle, a range of azimuthal angles could be selected (thus defining a cone of possible irradiation directions). For a fixed polar angle that results in a beam that just misses the lens, any given azimuthal angle will result in a dose gradient across the lens as a consequence of scatter radiation. By entering the eye from more than one azimuthal angle to deliver the same macula dose, this scatter dose gradient would be smeared out, thus minimizing the dose to any given edge of the lens. Based upon consultation with Oraya Therapeutics medical staff, a polar angle of 30° from the geometric axis was adopted in this study for lens dose avoidance.

The other important structure for dose avoidance is the optic nerve which, unlike the lens and macula, is not symmetric with respect to the beam azimuthal entry angle. The optic nerve is currently modeled as a cylindrical cuboidal structure tilted to the center of the patient's face by 20° (as per NCRP Report No. 130) so that some values of the vertical tilt angle might place the optic nerve directly within the path of the beam. Obviously, the vertical tilt angle of optic nerve is a crucial factor to determine clinically available beam directions. There is lack of literature on vertical tilt for this tissue and its possible variability within the adult patient population. Unsold *et al.*[28] reported that the optic nerve cannot be visualized in a single axial section of computed tomography because of its sinuosity and motility within the orbit. According to their investigation, the entire optic nerve appeared through axial planes from −20° to 0° with respect to the orbitomeatal baseline. Considering this lack of literature information and possible patient-dependent variability, a sensitivity study for the optic nerve vertical tilt was undertaken with a total of five different vertical tilt angles: +20°, +10°, 0°, −10°, and −20° all relative to the geometric axis.

An array of eight potential beam entry directions was envisioned and included in the MCNPX eye model as shown in Figs. 3(A) and 3(B), showing frontal and perspective views of eye model and beam entry directions, respectively. These angles can be described using a spherical 3D polar coordinate system with the macula at the origin and the z-axis defining the geometric axis. In all eight beam azimuthal angles, the source-to-target distance was assumed to be 13 cm, and the polar angle was fixed at 30° from the geometric axis. The azimuthal angle changes in eight increments of 45° in a clockwise fashion, such that an angle of 0° corresponds to the 12 o'clock position when viewing the patient's treated eye.

II.E. Verification of Monte Carlo simulation

Experiments were undertaken to verify the accuracy of MCNPX-based simulations of the incident x-ray energy spectrum and the ensuing photon interactions. A commercially available MXR160HP/11 x-ray tube (Comet AG, Switzerland) was used, powered by an XRV160N3000 generator (Spellman, Hauppauge, NY). The tube potential of 100 kVp and 1.25 mm Al filtration was added to that provided by a 0.8 mm thick Be window. A parallel plate ion chamber (Type 34013, PTW, Freiburg, Germany) connected to a UNIDOS E electrometer (PTW, Freiburg, Germany) was used to measure air kerma at 1 m from the anode. At a distance of 130 mm

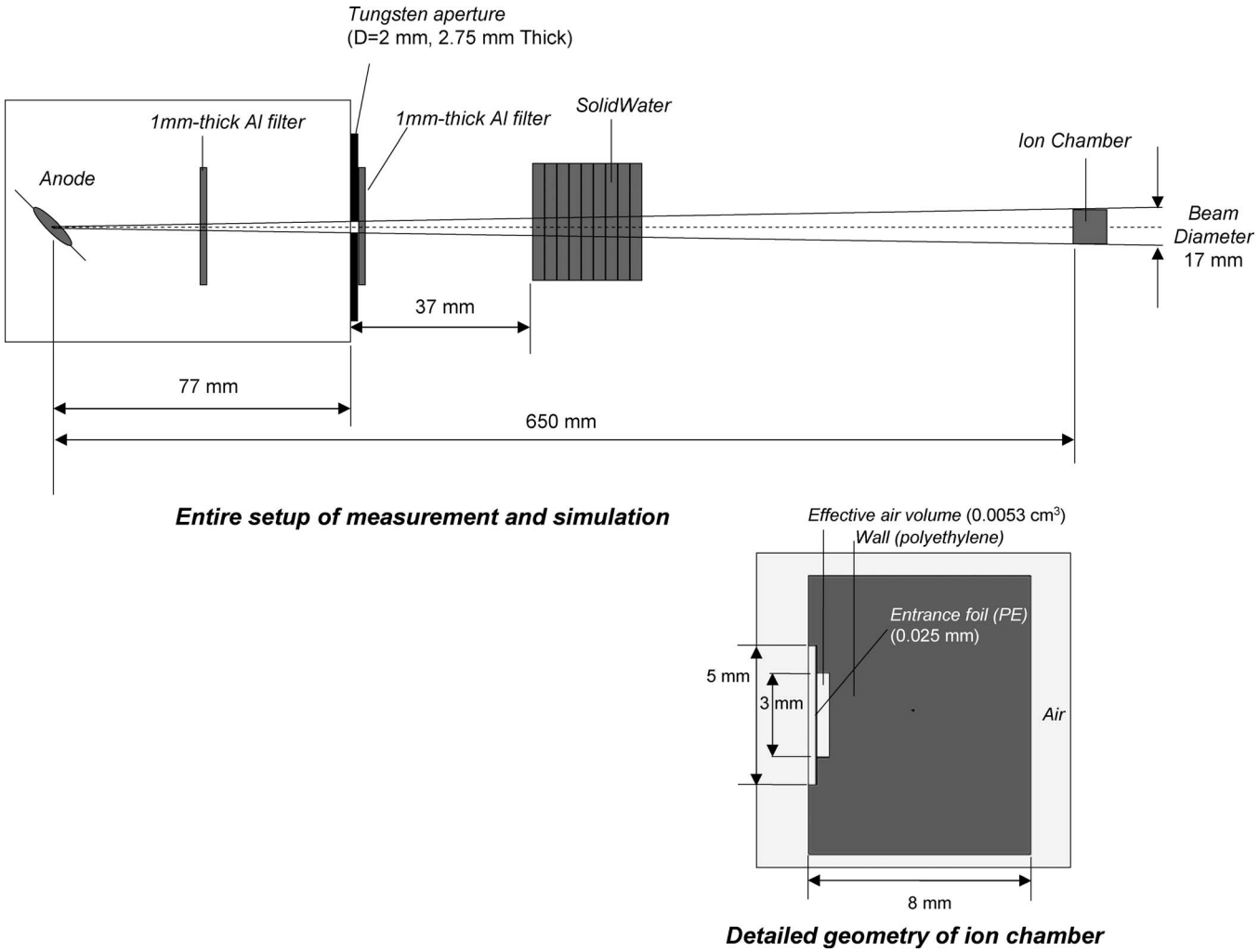

FIG. 4. Experimental setup of air kerma measurements along with a sagittal cross section of the MCNPX model of the ion chamber (Type 34013, PTW, Freiburg, Germany. A total of four materials were assigned to the ion chamber model: polyethylene entry foil, polyethylene wall, effective air volume, and surrounding air.

from the anode, a consecutive series of 2-mm-thick Solid Water panels (GAMMEX RMI, Middleton, WI) were placed within the primary beam to facilitate absorbed dose measurements as a function of depth within a water or soft tissue medium. Percent depth dose (PDD) relative to the surface dose was determined based on these measurements. The entire experimental setup was then simulated within MCNPX including the x-ray source, solid water phantom, and ion chamber. Simulated values of PDD were calculated through Monte Carlo radiation transport and compared with the experimental data. Fig. 4 shows the sagittal cross-section of the simulated ion chamber in MCNPX, which was generated by the MCNPX rendering tool.

II.F. Calculation of dose volume histogram

The mean absorbed dose to a given tissue structure within the eye does not give information regarding the dose distribution within that structure. These dose distributions were thus obtained using the Mesh Tally technique within MCNP to superimpose a cuboidal grid of small voxels over an existing geometrical structure within the eye model. The lens, macula, and optic nerve were modeled as an ovoid, a puckered disk, and a cylindrical cuboid, respectively. Accordingly, other than the optic nerve, it was not feasible to establish a mesh tally block, which would exactly encompass the lens and macula using existing MCNPX mesh-block shapes—rectangular, cylindrical, or spherical.[24] As an alternative approach, a rectangular mesh block was used to closely cover the lens and macula, and then a postprocessing MATLAB code was developed to selectively tabulate dose within the mesh voxels included within the true lens and macula geometrical boundaries. For the optic nerve, the mesh tally voxels were placed entirely within this tissue structure, and thus no post-processing was required for optic nerve DVH calculations. For each tissue structure, a mesh tally array of $20\times10\times20$ cells were created. The mesh cell sizes were set at $0.053\times0.042\times0.053$ cm^3 for the lens, $0.03\times0.01\times0.03$ cm^3 for the macula, and $0.01\times0.08\times0.01$ cm^3 for the optic nerve.

TABLE II. Comparison of percent depth dose from surface (%) between ion chamber measurements (mean and 1σ experimental error) and Monte Carlo simulations (mean and 1σ statistical error) for verification the MCNPX-based simulation model. A total 10^5 photon histories were considered in the simulation.

	Measurement		MC simulation		
Depth (mm)	Dose in 60 s (mGy)	Percent depth dose (%)	Dose per photon (mGy/photon)	Percent depth dose (%)	Rel Diff in PPD
0.0	99.59 ± 0.80%	100.0%	5.41E−20 ± 0.31%	100.0%	0.0%
2.2	90.51 ± 1.2%	90.9%	4.94E−20 ± 0.32%	91.4%	−0.5%
4.3	82.88 ± 1.1%	83.2%	4.55E−20 ± 0.33%	84.2%	−1.1%
6.5	76.38 ± 1.0%	76.7%	4.17E−20 ± 0.34%	77.1%	−0.6%
8.6	70.70 ± 1.4%	71.0%	3.85E−20 ± 0.35%	71.1%	−0.2%
10.8	64.74 ± 1.3%	65.0%	3.54E−20 ± 0.36%	65.5%	−0.7%
12.9	60.03 ± 1.2%	60.3%	3.25E−20 ± 0.37%	60.0%	0.4%
15.1	55.22 ± 1.2%	55.4%	3.00E−20 ± 0.38%	55.5%	0.0%
17.2	51.12 ± 1.1%	51.3%	2.78E−20 ± 0.39%	51.3%	0.0%
19.4	48.00 ± 1.1%	48.2%	2.58E−20 ± 0.40%	47.7%	1.1%
21.5	44.31 ± 1.1%	44.5%	2.40E−20 ± 0.41%	44.3%	0.4%
23.7	41.16 ± 1.0%	41.3%	2.22E−20 ± 0.43%	41.1%	0.6%
25.8	38.46 ± 1.0%	38.6%	2.08E−20 ± 0.44%	38.4%	0.6%
28.0	35.57 ± 1.0%	35.7%	1.92E−20 ± 0.45%	35.6%	0.4%

Once the mesh was established, radiation transport was simulated and voxel absorbed doses were obtained (approximated as tissue kerma in this study)[24] Given this array of data, the fractional volumes of target tissue that receive an absorbed dose greater than a specified value from zero to the maximum absorbed dose seen in that substructure were determined. This resulting histogram—a cumulative dose volume histogram—was used as the primary output format in this study for both targeted and non-targeted tissues.

III. RESULTS AND DISCUSSION

III.A. Depth dose verification in water phantom

Table II compares the theoretical MCNPX-based percent depth dose (PPD) in water with values experimentally measured for an x-ray spectrum at 100 kVp tube potential and with 1.25 mm Al and 0.8 mm Be total filtration. The MCNPX statistical errors were within 1%. Experimental values are given as the mean and the measurement uncertainty. The latter is taken for two effects in quadrature: the standard error of triplet measurements, and the error due to uncertainties in the thickness of the solid water slabs. Values of PDD are shown to differ not more than ~1.1% at depth.

III.B. Available beam angles for varying optic nerve vertical tilt angles

Considering the absence of definitive literature information on mean values of optic nerve vertical tilt (relative to the geometric axis), as well as possible patient-to-patient variations in this parameter, a sensitivity study was undertaken with a total of five different optic nerve tilt angles: −20° (maximal caudal tilt), −10°, 0° (lying within the geometric axis), +10°, and +20° (maximal cranial tilt). In Fig. 5, we plot the mean absorbed dose for the lens, optic nerve (function of vertical tilt angle), and macula target (fixed at 8 Gy per treatment beam) for a 100 kVp x-ray source a 2 mm Al total filtration. The mean dose to the lens was found be insignificant (51–53 μGy) for all beam directions and optic nerve tilt angles. Mean optic nerve doses were also found be insignificant (47–92 μGy) for all vertical tilt angles, and for treatment beam azimuthal angles between 0° and 180°.

For optic nerve vertical tilt angles of +10° or −10°, mean doses of approximately 1.6–1.7 Gy are seen for treatment beams 225° or 315°, respectively. At optic nerve vertical tilt angles at their extreme values (±20°), mean optic nerve doses are shown to be reduced at around 0.80–0.85 Gy per treatment. If the patient's optic nerve is within the geometric axis (0° vertical tilt), a maximal mean absorbed dose of up to 4.9 Gy is predicted in the current model for a treatment beam entrance angle of 270°, where this tissue would be directly within the lateral path of the x-ray beam.

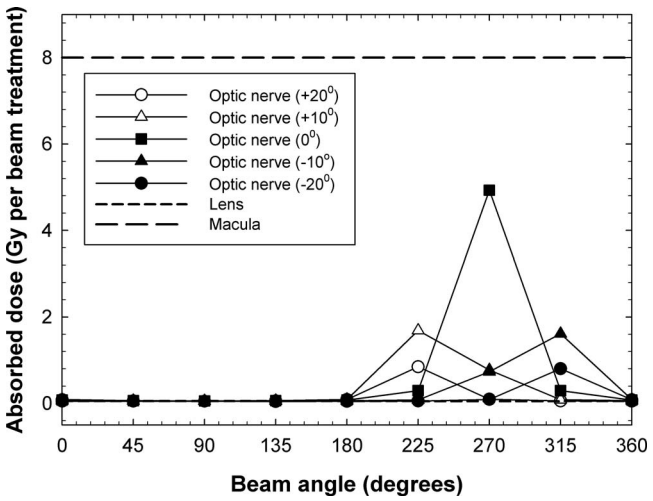

FIG. 5. Mean absorbed dose (Gy) to the macula, lens, and optic nerve as function of treatment beam azimuthal entry direction (0°–360°) and assumed vertical tilt angle of the patient's optic nerve (from +20° to −20°) in the cranial (+) to caudal (−) direction.

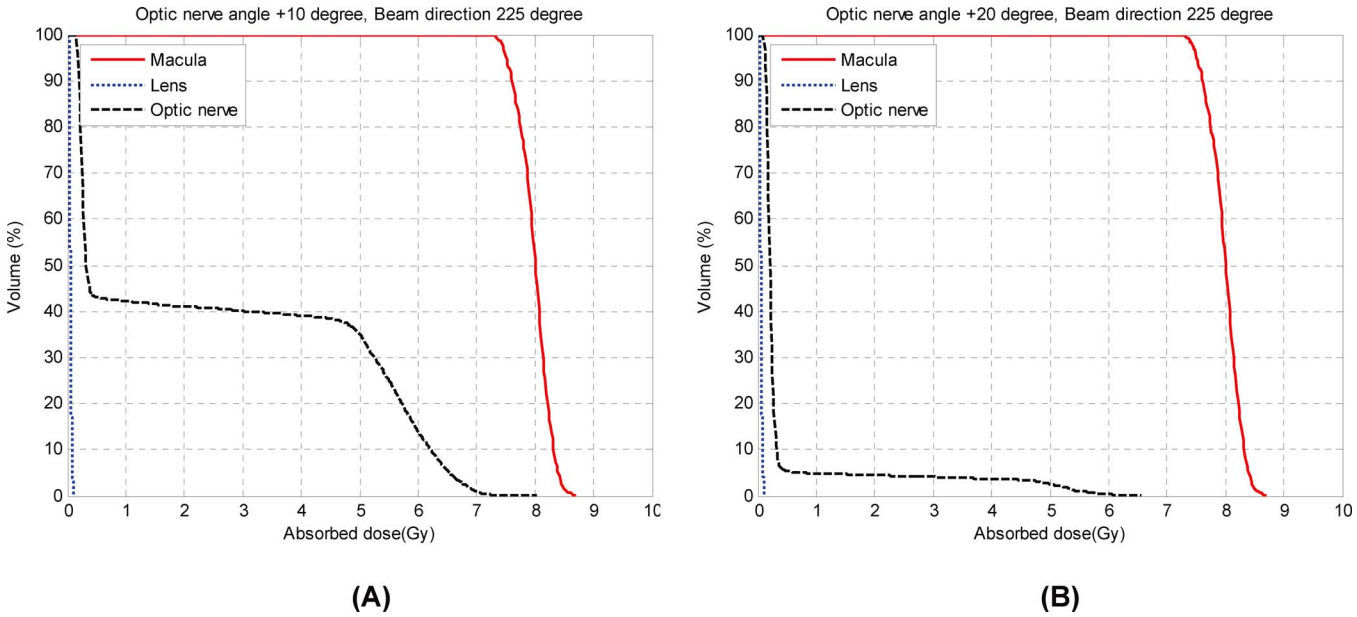

FIG. 6. Dose volume histograms for the macula target, the lens, and optic nerve when (**A**) optic nerve vertical tilt angle was +10° and (**B**) optic nerve vertical tilt angle was +20°. In both cases, the azimuthal beam entry direction was set at 225° as per Fig. 3.

More clinically relevant data regarding normal tissue complications, however, are given in the form of a dose–volume histogram as shown in Figs. 6(A) and 6(B). Here, the DVHs for optic nerve vertical tilt angles of +10° and +20° were calculated for a treatment beam azimuthal angle of 225° Figure 6(A) shows the DVH for a vertical tilt angle +10°, where about 40% of optic nerve volume is shown to receive absorbed doses of more than 5 Gy. When the optic nerve is set at +20° to the geometric axis, however, only ~5% of its volume receives an absorbed dose exceeding 5 Gy as shown in Fig. 6(B). The modeling data thus demonstrates that the treatment beam azimuthal angle 225° is potentially a viable therapy option if the patient's optic nerve is orientated within or caudal to the geometric axis as indicated in data by Unsold *et al.*[28] Accordingly, at the present time, three azimuthal beam treatment angles are being considered in preclinical trials—135°, 180°, and 225°—given dosimetric, clinical, and technical considerations of beam delivery and patient setup. Although beam treatment angles less than 135° are dosimetrically favorable, they were not considered further in the prototype design due to limitations of beam delivery with respect to equipment setup and facial bony anatomy.

III.C. Dependence of dose volume histograms on beam energy

To investigate the dependence of the macula dose on beam energy, DVHs for the macula, lens, and optic nerve were calculated for three different tube potentials (80, 100,

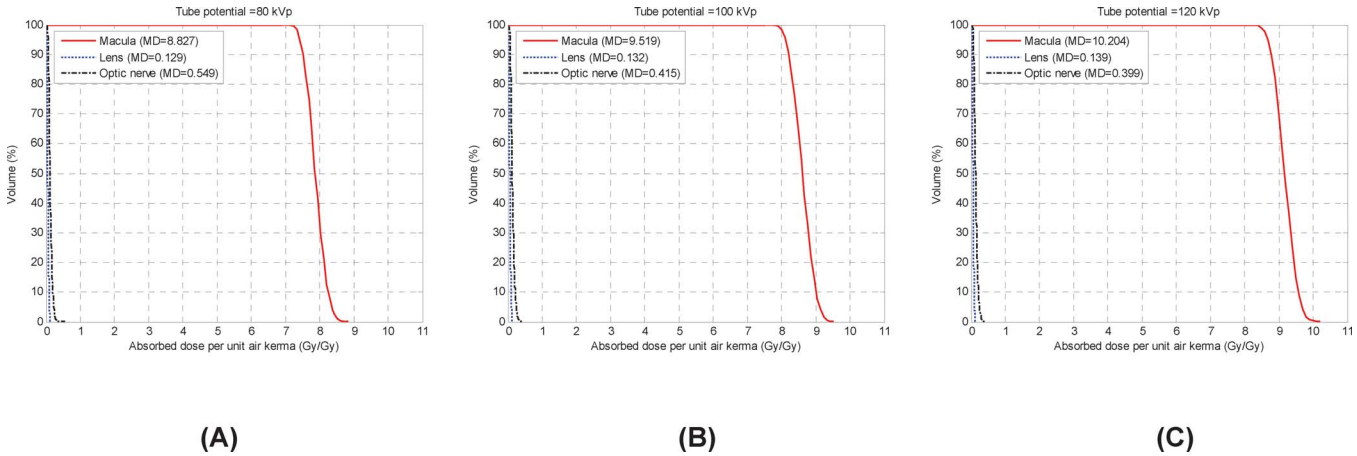

FIG. 7. Dose volume histograms (dose per unit air kerma) for the macula target, the lens, and optic nerve for three different x-ray energy spectra: 80, 100, and 120 kVp. The maximum dose per unit air kerma is provided in the legend of each plot for all targets. Additional assumptions are an optic nerve vertical tilt angle of 0° and a beam entrance azimuthal angle of 180°.

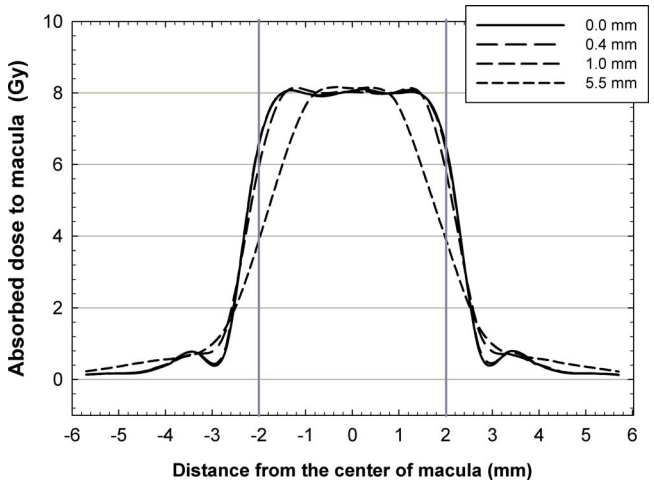

FIG. 8. Cross-sectional profile of the absorbed dose to the macula target for a 100 kVp x-ray beam as a function of focal spot size. Vertical lines are placed at +2 and −2 mm, thus, outlining the geometric dimensions of the 4-mm diameter macula target. To simply the MCNP geometrical setup, a nonclinical normally incident beam angle is assumed (polar angle set at 0°).

and 120 kVp) and are depicted in Figs. 7(A)–7(C), respectively. The patient's optic nerve is assumed to be at 0° vertical tilt (within the geometric axis), and the treatment beam azimuthal angle is fixed at 180°. In these plots, abscissa values are given, not as absolute tissue dose, but as a dose coefficient in units of Gy/Gy—absorbed dose per unit air kerma measured free-in-air at 100 cm from the x-ray source. The maximum dose coefficient is additionally provided in the legend of each plot for all targets. In Fig. 7, we note that in moving from 80 kVp in Fig. 7(A) to 120 kVp in Fig. 7(C), the maximum dose coefficient to the target increases by 16% from 8.8 to 10.2 Gy/Gy as expected due to the higher tissue penetration of the x-ray beam. As a result, only 86% of the integrated tube current (mAs) is required at the higher energy for target dose delivery. The lens and optic nerve dose coefficients are significantly lower than seen for the macula target at all energies. In Fig. 7(B) for example, the maximal lens and optic nerve dose coefficients are lower than the maximal macular target dose coefficient by factors of ~72 and ~23, respectively.

III.D. Dependence of dose volume histograms on focal spot size

An additional study was performed regarding the influence of the x-ray source focal spot size on the resulting dose profile across the macula target volume. In Fig. 8, absorbed dose profiles at the center of macula are shown for focal spot sizes of 0.0, 0.4, 1.0, and 5.5 mm, respectively, for a targeted central dose of 8 Gy. Vertical lines represent the anatomic size of the target at 4 mm diameter. No significant differences in the dose profile are seen for focal spot sizes from 0.0 to 1.0 mm, and the penumbra of each extends outward 1 of 2 mm radially. For the larger 5.5 mm spot size, dose uniformity is significantly reduced within the target region, such that the dose at the edges of the target are only one-half that at center, and the penumbra extends outward at slightly higher dose values than seen for the smaller spot sizes. Dose coefficients in the central region were estimated to be 7.8, 7.7, and 7.7 Gy/Gy for spot sizes of 0, 0.4, and 1.0 mm, respectively, where the reference air kerma value is again set at 100 cm from the x-ray source. The dose coefficient for the 5.5 mm spot size beam is 18 Gy/Gy, thus requiring only ~42% of the integrated tube current (mAs) needed to deliver 8 Gy central dose using the smaller focal spot sizes. However, its dose uniformity is significantly reduced within the macula target.

IV. CONCLUSIONS

A new approach for radiation treatment of ARMD has been developed to provide a new treatment option for this disease. To provide an understanding of the dosimetry characteristics of this approach, a parametric Monte Carlo simulation study was undertaken. A 3D eye model with major substructures was carefully designed based on the anatomy and dimensional data reported in NCRP Report No. 130. The model was then used within the MCNPX2.5 radiation transport code to investigate available beam geometries for ARMD treatment, the effect of tube potential and focal spot size on target and nontarget doses, and volumetric distribution of absorbed dose within these same tissues.

Given the study results presented here, several recommendations can be made with regard to the use of collimated x-ray beams for treatment of ARMD. The goal of the treatment is to deliver 24 Gy to the macula (as per the NeoVista Study Group results) simultaneously delivering the lowest possible dose to nontarget tissues, preferably below thresholds that cause deleterious effects. The primary nontarget tissues of concern are the lens and optic nerve. Based on the calculation of absorbed dose and DVH for different beam directions and optic nerve tilt angles in this initial eye model, as well as technical and anatomic issues regarding beam delivery, treatment beam azimuthal angles of 135°, 180°, and 225° would potentially be available for prototype development and preclinical testing A mean dose of 8 Gy to the macula in each of the three beam directions would thus deliver a cumulative absorbed dose of 24 Gy to macula. For a fixed tube current, the target dose delivered at 120 kVp will be about 16% higher than that delivered at 80 kVp. There is no significant difference in dose profile across the macula for focal spot sizes of 0.0, 0.4, and 1.0 mm, whereas severe nonuniformity of target dose, and an slightly larger penumbra dose is expected at a focal spot size of 5.5 mm.

Not considered in the present model are nontarget doses to the brain, especially the tissues of the frontal lobe receiving the highest exposure. The focused x-ray beams will penetrate the orbital bone and irradiate the anterior regions of the brain for all possible treatment entry angles. Detailed dose profiles in various brain tissues should be examined with the intent of further selecting beam angles that minimize dose to critical structures. The research team is currently investigating the use of a realistic computational head phantom described by nonuniform rational B-spline surfaces and based upon normal patient computed tomography head images.[29,30]

Coupled with this model development effort are companion studies to (1) further characterize nonsymmetric positioning of the macula target relative to the geometric axis, and (2) measure and characterize the 3D anatomical shape and position of the optic nerve within the adult male and female patient population. This latter feature has been shown in this study to be crucial to the selection of optimal treatment beam angles, and to the avoidance of optic nerve tissue complications.

ACKNOWLEDGMENT

This study was conducted at the University of Florida (UF) and at the University of Medicine and Dentistry of New Jersey (UMDNJ) under financial support from Oraya Therapeutics, Inc. of Newark, CA.

[a]Author to whom correspondence should be addressed. Electronic mail: wbolch@ufl.edu; Telephone: (352) 846-1361; Fax: (352) 392-3380.

[1]H. Churei, K. Ohkubo, M. Nakajo, H. Hokotate, Y. Baba, J. Ideue, K. Miyagawa, H. Nakayama, Y. Hiraki, T. Kitasato, and N. Yabe, "External-beam radiation therapy for age-related macular degeneration: two years' follow-up results at a total dose of 20 Gy in 10 fractions," Radiat. Med. **22**, 398–404 (2004).

[2]R. P. Murphy, "Age-related macular degeneration," Ophthalmology **93**, 969–971 (1986).

[3]N. M. Bressler, S. B. Bressler, and S. L. Fine, "Age-related macular degeneration," Surv. Ophthalmol. **32**, 375–413 (1988).

[4]B. Morris, F. Imrie, A. M. Armbrecht, and B. Dhillon, "Age-related macular degeneration and recent developments: new hope for old eyes?," Postgrad Med. J. **83**, 301–307 (2007).

[5]Macular Photocoagulation Study Group, "Visual outcome after laser photocoagulation for subfoveal choroidal neovascularization secondary to age-related macular degeneration. The influence of initial lesion size and initial visual acuity," Arch. Ophthalmol. (Chicago) **112**, 480–488 (1994).

[6]VPT Study Group, "Photodynamic therapy of subfoveal choroidal neovascularization in pathologic myopia with verteporfin. 1-year results of a randomized clinical trial--VIP report no. 1," Ophthalmology **108**, 841–852 (2001).

[7]P. J. Rosenfeld, D. M. Brown, J. S. Heier, D. S. Boyer, P. K. Kaiser, C. Y. Chung, and R. Y. Kim, "Ranibizumab for neovascular age-related macular degeneration," N. Engl. J. Med. **355**, 1419–1431 (2006).

[8]A. Capone and Macugen AMD Study Group, "Intravitreous pegaptanib sodium (Macugen) in patients with age-related macular degeneration (AMD): Safety and pharmacokinetics," Invest. Ophthalmol. Visual Sci. (Annual Meeting Abstracts) Online **46**, E-Abstract 2362 (2005).

[9]I. Crocker, T. Ciulla, E. Butker, G. Burian, and B. Hubbard, "Initial experience with Therasight ocular brachytherapy system for treatment of ARMD," Radiother. Oncol. **75**, S58–S59 (2005).

[10]G. Hubbard, S. Carr, K. Millage, and R. Waldron, "Cadaver evaluation of a new ocular brachytherapy system," Invest. Ophthalmol. Visual Sci. **45**, 5139 (2004).

[11]J. S. Heier, "Concomitant therapy of epiretinal radiation and bevacizumab for neovascular AMD," in *2007 Annual Meeting of the American Academy of Opthalmology*, New Orleans, LA (2007).

[12]H. J. Zambarakji, A. M. Lane, E. Ezra, D. Gauthier, M. Goitein, J. A. Adams, J. E. Munzenrider, J. W. Miller, and E. S. Gragoudas, "Proton beam irradiation for neovascular age-related macular degeneration," Ophthalmology **113**, 2012–2019 (2006).

[13]A. Haas, G. Papaefthymiou, G. Langmann, O. Schrottner, B. Feigl, K. A. Leber, R. Hanselmayer, and G. Pendl, "Gamma knife treatment of subfoveal, classic neovascularization in age-related macular degeneration: a pilot study," J. Neurosurg. **93**, 172–176 (2000).

[14]M. Hayashi, M. Chernov, M. Usukura, K. Abe, Y. Ono, M. Izawa, S. Hori, T. Hori, and K. Takakura, "Gamma knife surgery for choroidal neovascularization in age-related macular degeneration. Technical note," J. Neurosurg. **102**, 200–203 (2005).

[15]M. A. Henderson, S. Valluri, S. S. Lo, T. C. Witt, R. M. Worth, R. P. Danis, and R. D. Timmerman, "Gamma knife radiosurgery in the treatment of choroidal neovascularization (wet-type macular degeneration)," Stereotact. Funct. Neurosurg. **85**, 11–17 (2007).

[16]D. M. Marcus, E. Peskin, M. Maguire, D. Weissgold, J. Alexander, S. Fine, and D. Followill, "The age-related macular degeneration radiotherapy trial (AMDRT): One year results from a pilot study," Am. J. Ophthalmol. **138**, 818–828 (2004).

[17]RAD Study Group, "A prospective, randomized, double-masked trial on radiation therapy for neovascular age-related macular degeneration (RAD Study). Radiation Therapy for Age-related Macular Degeneration," Ophthalmology **106**, 2239–2247 (1999).

[18]S. V. Goverdhan, F. A. Gibbs, and A. J. Lotery, "Radiotherapy for age-related macular degeneration: no more pilot studies please," Eye **19**, 1137–1141 (2005).

[19]F. Schwarz and D. Christie, "Use of 'sham' radiotherapy in randomized clinical trials," J Med Imaging Radiat Oncol **52**, 269–277 (2008).

[20]NCRP, "Biological effects and exposure limits for hot particles," Report No. 130, National Council on Radiation Protection and Measurements, Bethesda, MD (1999).

[21]C. A. Girkin, C. H. Comey, L. D. Lunsford, M. L. Goodman, and L. B. Kline, "Radiation optic neuropathy after stereotactic radiosurgery," Ophthalmology **104**, 1634–1643 (1997).

[22]S. L. Stafford, B. E. Pollock, J. A. Leavitt, R. L. Foote, P. D. Brown, M. J. Link, D. A. Gorman, and P. J. Schomberg, "A study on the radiation tolerance of the optic nerves and chiasm after stereotactic radiosurgery," Int. J. Radiat. Oncol., Biol., Phys. **55**, 1177–1181 (2003).

[23]R. P. Singh, D. Moshfeghi, E. M. Shusterman, S. A. McCormick, and M. Gernter, "Evaluation of transconjunctival collimated external beam radiation for age-related macular degeneration (ARMD) [abstract]," in *2008 Annual Meeting of the American Academy of Opthalmology*, Atlanta, GA, 2008, pp. 08-PP-30018701-AAO.

[24]D. B. Pelowitz, *MCNPX User's Manual Version 2.5.0*, LA-CP-05-0369. (Los Alamos National Laboratory, Los Alamos, NM, 2005).

[25]K. Cranley, B. J. Gilmore, G. W. A. Fogarty, and L. Desponds, "Catalogue of diagnostic x-ray spectra and other data," Report No. 78, The Institute of Physics, London, UK 1997.

[26]M. Cristy and K. F. Eckerman, "Specific absorbed fractions of energy at various ages from internal photon sources," ORNL/TM-8381/Volumes I-VII, Oak Ridge National Laboratory, Oak Ridge, TN, 1987.

[27]ICRU, "Photon, electron, proton and neutron interaction data for body tissues," Report No. 46, International Commission on Radiation Units and Measurements, Bethesda, MD, 1992.

[28]R. Unsold, J. DeGroot, and T. H. Newton, "Images of the optic nerve: anatomic-CT correlation," AJR, Am. J. Roentgenol. **135**, 767–773 (1980).

[29]C. Lee, C. Lee, D. Lodwick, and W. E. Bolch, "NURBS-based 3D anthropometric computational phantoms for radiation dosimetry applications," Radiat. Prot. Dosim. **127**, 227–232 (2007).

[30]C. Lee, D. Lodwick, J. L. Williams, and W. E. Bolch, "Hybrid computational phantoms of the 15-year male and female adolescent: applications to CT organ dosimetry for patients of variable morphometry," Med. Phys. **35**, 2366–2382 (2008).